J Mater Sci

Chemical routes to materials

Silk fibroin protein as dual mode picric acid sensor and UV photoactive material

Indranee Hazarika[1], Kangkan Jyoti Goswami[2,3], Amreen Ara Hussain[4], Tapash Kalita[1], Neelotpal Sen Sarma[2,3,*], and Bedanta Gogoi[1,*]

[1] *Department of Chemistry, Gauhati University, Jalukbari, Guwahati-14, Assam, India*
[2] *Advanced Materials Laboratory, Institute of Advanced Study in Science and Technology, Paschim Boragaon, Guwahati-35, Assam, India*
[3] *Academy of Scientific and Innovative Research (AcSIR), Ghaziabad 201002, India*
[4] *Facilitation Centre for Industrial Plasma Technologies (FCIPT), Institute for Plasma Research (IPR), Gandhinagar 382428, Gujarat, India*

Received: 17 June 2021
Accepted: 1 September 2021

ABSTRACT

Silk fibroin (SF) protein was reported as a versatile platform for selective detection of picric acid (PA) as well as for UV photodetection. SF in aqueous media undergoes about 74% fluorescence quenching in the presence of 24 nM concentration of PA in aqueous media with a limit of detection of about 0.203 nM. The quenching was found to due to the combined effect of Förster resonance energy transfer, hydrogen-bonding, and electrostatic interaction. The method is also applicable for real environmental samples. Electrical measurement-based sensing of PA was also performed by fabricating flexible sensor devices from SF and polyvinyl alcohol on polyethylene terephthalate substrates. The sensors show about twofold enhancement in current conduction and about 33% higher ionic conduction in the presence of the analyte. Interestingly, the combination of SF and PA acts as a photoactive material for UV light and generates about 7.15 μA photocurrent under 360 nm light-emitting diodes. The devices exhibit excellent stability in repetitive bending of the devices and also air-stability at varying relative humidity conditions (40–80%). Additionally, an electronic circuit was designed for precise electrical parameters required during optoelectronic measurements. Therefore, it can be stated that, SF can be used as a versatile platform for dual mode PA sensor as well as UV photodetector.

Handling Editor: Pedro Camargo.

Indranee Hazarika and Kangkan Jyoti Goswami have equally contributed to this work.

Address correspondence to E-mail: neelot@iasst.gov.in; bedanta@gauhati.ac.in

https://doi.org/10.1007/s10853-021-06506-9

Published online: 18 September 2021

Introduction

Picric acid (PA) or 2, 4, 6- Trinitrophenol is a common nitroaromatic compound [1] and is widely employed in making deadly weapons, rocket fuels, fireworks, matches, dyes, pharmaceutics [2]. Wide use and disposal of this water soluble compound increases the possibility of environmental pollution. In addition to this, it is also hazardous in case of skin and eye contact, ingestion, or inhalation [3]. Therefore, it is important to detect the presence PA in real environmental samples. However, in the real-world scenario, the detection of PA is done in a much more complex environment than the controlled experiments conducted in laboratories [4, 5]. For example, such chemicals are deposited on the explosion sites and mixed with soil and other chemicals. In addition, the mixture of explosive materials is used to make real explosives. The sensor system should also work in aqueous media for the real sample analysis. In such circumstances, it is quite a challenge to selectively detect PA from real samples. Other technical limitations related to such detection processes is the use of sophisticated instrumentations such as X-ray diffraction, surface enhanced Raman Spectroscopy, gas chromatography-mass spectrometry, etc.[6], which is available only in certain institutions and also not possible to use in actual explosion sites. The preparation of efficient sensory materials with active sites that react particularly to PA is another challenge to the researchers and requires multistep reaction protocol which increases the cost of production. Therefore, now a days fluorescence-based PA sensors are widely used to address these issues to some extent because of their cost effectiveness, high sensitivity, and quick response. [7, 8]

In this work, we report the silk fibroin (SF) as a chemosensor for the selective detection of PA. SF is the major constituent of silk fiber which serve as the inner core and provide mechanical strength to the fiber. It is coated with a glue like protein called sericin which has to be removed using the standard protocol. [9, 10] Because of the excellent biological properties, SF is extensively used in biomedical applications such as biosensors, [11] wound dressing, [12] in drug delivery, [13] tissue engineering, [14] etc. However, its optoelectronic properties are relatively unexplored. To the best of our knowledge, this is the first attempt to use this biopolymer to develop dual sensor for PA using fluorescence as well as electrical methods with a better limit of detection (LOD) and selectivity. Flexible and portable devices were also fabricated using facile fabrication techniques for electrical measurements. More interestingly, it was found that, the combination of SF and PA emerge as a potential candidate for ultra violet (UV) photodetector device fabrication as it shows the characteristic increment of current conduction or photocurrent generation under UV light emitting diode (LED). The underlying photophysical mechanisms behind such observation in semiconducting materials is a fascinating topic and in the past, researchers have established the occurrence of different energy transfer and charge transfer mechanisms involved in the sensing as well as optoelectronic measurements. In the current context, Förster resonance energy transfer (FRET) is confirmed as the mechanism of energy transfer between the donor and the acceptor material that increase the fluorescence quenching efficiency as well as the photocurrent of the devices. Before going into the details of the photodetector devices, let's have an idea about the importance of photodetectors and the common materials used in optoelectronics to understand the importance of using biological materials to develop the same.

An enormous amount of effort is being made by the scientific community in the ground of optoelectronics that provides a stronger foundation to the architecture of information technology of a country, which, in turn, directly impact the everyday life, economic growth as well as national security. Advancements in photodetectors play a vital role in this ground for its wide range of applications, such as in communication devices, remote sensing, national security, detecting harmful radiations, and environmental sensing like detecting pollutants, health monitoring, night surveillance, etc. [15–17]. Inorganic semiconducting materials are predominantly used in this area due to their robustness and superior photophysical properties. In the literature, it was found that a variety of materials from organic, inorganic, organic–inorganic hybrid materials, different nanostructured materials have been extensively used for fabricating photodetector devices. Out of the inorganic materials, photodetectors based on p-n heterojunctions are fabricated using various n-type (TiO_2,[18] ZnO [19], SnO_2,[20] Zn_2SnO_4,[21] Zn_2GaO_4,[22] Zn_2GeO_4,[23] ZnS[24], $Ga_2In_4S_9$ [25]) and p-type (GaN [26], SiC [27], NiO [28],) metal oxides.

Additionally, the organic materials such as 2-(1,10:30,100-triphenyl-50-yl)-9,9-diphenyl-9H-fluorene (TPF) and (9,9-diphenyl-9H-fluoren-2-yl)diphenylphosphine oxide (DFPPO)[29], conducting polymers [30], etc. are also highlighted in photodetectors. Recently, the perovskite structures have also drawn considerable attention based on their remarkable photoresponse in optoelectronic devices. For instance, the double perovskites Cs_2TeI [31], organic–inorganic halide perovskites [32], lead-free perovskites [33–36], have shown impressive photoresponses. Several graphene-based optoelectronics devices are also widely explored due to excellent conductivity and flexibility [37–39]. Other than these materials, nanoparticles, quantum dots, carbon dots are extensively used in fabricating optoelectronic devices [40–42]. On the other hand, photoconductive devices based on various photoactive materials such as PbS colloidal quantum dots [43], GeSn/Ge multiple-quantum-well [44], black phosphorous/Indium Selenide [45], Bi_2Te_3,[46] etc. are reported to be simple yet efficient photodetectors in recent years.

Although all these materials show excellent photophysical properties, their synthesis protocol is not straightforward. Also, device fabrication processes using such materials involve sophisticated instruments and require interfacial supporting layers such as electron transport layers (ETL) and hole transport layers (HTL) to increase the efficacy of the devices making the devices quite expensive to fabricate and use. Many of these materials also reported to be harmful to human health and the environment. In this work, to address the importance of designing low-cost photodetectors and the use of non-toxic materials, we investigated the basic photodetector characteristics of naturally available SF protein-based simple optoelectronic devices that do not require other supporting materials such as ETL and HTL for preliminary photodetection experiments. The adhesion properties of the SF on different substrates also ensure better contact between the photoactive material with the electrodes [47]. This will prevent charge carrier recombination during the electrical measurements. Unlike the heterojunction-based photodetectors, the devices designed in this work are photoconductors that develop electrical current under UV light irradiation due to donor–acceptor mechanism. Photoconductive photodetectors are reported to be low-cost alternatives to the heterojunction-based optoelectronic devices. Such devices are easier to fabricate since they are fabricated using only the photoactive material with a pair of metal contacts [48].

In our previous works, detection of PA using bio-based conjugates were investigated. [7, 49] The synthesis process of these conjugates was not straightforward and also the limit of detection (LOD) were relatively higher. In the current work, naturally available starting material were extracted with improved LOD of PA sensing. It provides a versatile platform for PA as well as UV light detection under ambient conditions. We believe that the findings of this work will open up research in the direction of using SF-based optoelectronic devices for cost-effective technology development. The strategy used for developing PA sensor and photodetection by using SF is shown in Scheme 1.

Experimental section

Materials

PA was purchased from SIGMA, ortho-nitropheneol, meta-nitrophenol, para-nitrophenol were purchased from Merck, and LiBr, PVA with average molecular weight of 1,15,000 were purchased from LOBA CHEMIE. All the chemicals were used without further purification. SF was extracted from Eri silk fibers (Samia Cynthia).

Caution! PA is a hazardous chemical and has to be stored in 50% water (W/V). All the safety measures such as its use in very small quantities, wearing personal protective equipment, vacuum drying should be taken while handing PA. According to the US OSHA (United States Occupational Safety and Health Administration) and US NIOSH (United States National Institute for Occupational Safety and Health), the permissible exposure limit of PA is 0.1 mg/m^3.

Extraction of SF

In an aqueous solution of 0.02 M $NaHCO_3$, 3.04 g of cleaned silk cocoon were heated at 100 °C for one hour with continuous rotation. Then, it was thoroughly rinsed with warm water. The degummed silk fibers were dried at 60 °C and stored in vacuum desiccator [50]. Finally, the degummed silk fibers (0.2 g) were dissolved in 20 mL of 9 M solution of

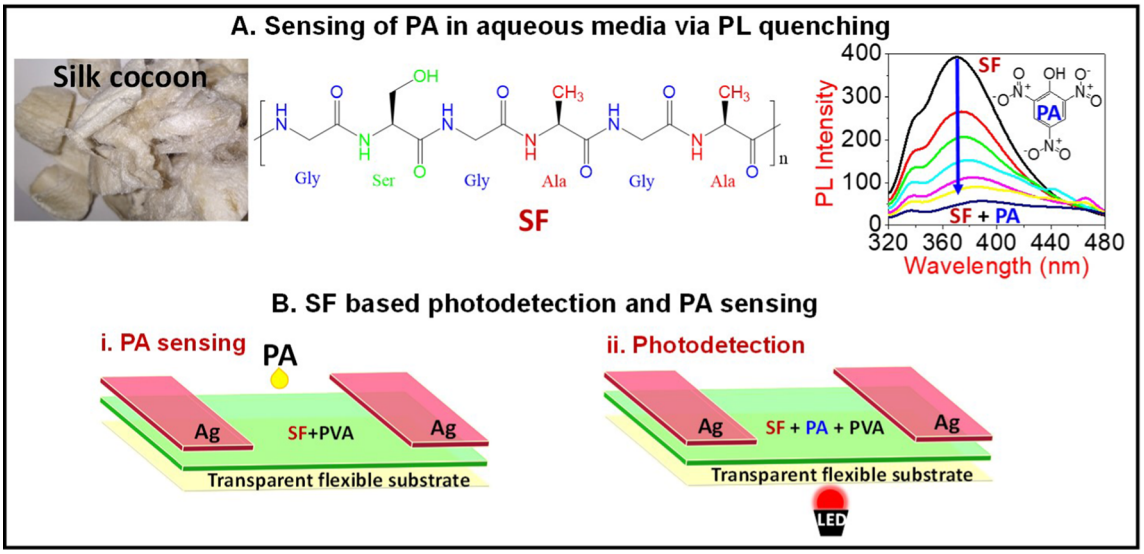

Scheme 1 Schematic representation of **a** Sensing of PA in aqueous media using SF as the fluorescence probe, **b** Device architectures for PA sensing and photodetection.

LiBr to get a saturated solution and stored in the refrigerator. This stock solution was further diluted to prepare 10% (V/V) solutions and all the experiments were performed using this solution. In general procedure of extracting SF, LiBr is removed from the solution using a dialysis process, but in our case device fabrication would be done in the later stages for electrical measurements. Hence, the presence of LiBr would help in facilitating better current conduction in the devices. Additionally, without the dialysis step, the process becomes easier, less time consuming, and cost-effective. The SF so prepared is stable upto two months and can be used for sensing experiments for this period.

Characterization techniques

Fourier transform infrared (FT-IR) spectra were recorded using PerkinElmer FT-IR spectrophotometer in transmission mode over 32 scans in the range 500 to 4000 cm^{-1}. For FT-IR spectroscopic analysis, samples were mixed with KBr to make pellets stored in a vacuum desiccator before recording the spectra. UV–vis absorption spectra were recorded by using SCHIMADZU-1800 spectrometer and the Photoluminescence (PL) emission spectra with various excitation wavelengths were recorded by using the Hitachi F-2500 spectrophotometer. For both the UV–vis absorption and photoluminescence (PL) measurements, quartz cuvettes of 1 cm path length were used. Fluorescence lifetime of the samples in aqueous media were measured using Edinburg instruments FSP920, Picosecond Time-resolved cum Steady State Luminescence Spectrometer. A LASER source of wavelength 300 nm was used as the excitation source. The zeta potential of the samples in aqueous media was determined using a Malvern Nano ZS90 Zetasizer. Surface morphology of the SF protein, and the films were characterized with the help of scanning electron microscope (∑IGMA^{TM} Field Emission Scanning Electron Microscope) and atomic force microscope (Nanosurf CoreAFM). For SEM measurements, the silk fibers were placed on a carbon tap and the films were drop casted on silicon wafers. Gold coating was done over all the samples with the help of a sputtering unit. For the AFM measurements, the films were drop casted over poly-(ethylene terephthalate) (PET) substrates and the images were recorded using non-contact mode. The electrical characterization of the device was performed using KEITHLEY 6517b electrometer.

Methods

Sensing experiments via fluorescence measurements

To investigate the fluorescence response of the SF protein toward PA in aqueous media, two milliliters of the 10% SF (V/V) was transferred into a quartz cuvette (4 × 1 × 1 cm) and the fluorescence spectra were recorded at an excitation wavelength (λ_{ex}) of

300 nm. To this, nanomolar concentration of PA with increasing concentration was added and the change in the fluorescence response was recorded. To mimic the sensing experiments for real sample analysis, tap-water and soil-water were simply filtered and spiked with PA and the fluorescence response of SF was recorded using the same experimental parameters. In a similar manner, the interference of common salts toward the sensing of PA was also investigated.

Device fabrication for sensing experiments and for investigating photocurrent generation

A cost-effective route and a simple device fabrication process has been adapted for the sensing of PA using electrical measurements as well as for UV photodetection. For the former, 10% SF (V/V) was mixed with 8% poly-vinyl alcohol (PVA) (W/V) in water and a fixed volume of 100 µL was deposited on thin transparent PET sheets by drop casting method followed by heating in a hot air oven at 60 °C overnight. Silver paste (Ag) with similar surface area (0.5 × 1) cm^2 were deposited at the two ends of the thin film. The area in between the two Ag-electrodes was fixed at 1 cm^2. To investigate the photoactivity of the donot-acceptor combination, the same procedure of device fabrication has been followed, except the remaining solution of the fluorescence sensing experiment that showed highest quenching was mixed with 8% PVA (W/V) solution and then deposited on PET substrate. The device architecture is shown in Scheme 1b. The idea behind using 8% PVA (W/V) solution is to ensure better contact between the materials and the electrodes. It also provides a stretchable substrate required in performing experiments at different bending angles. Also, in case of the device fabricated on PET substrates, the PVA film helps bind the photoactive material during measurements at different bending angles. All the devices were stored in a vacuum desiccator. For photodetection experiments, we used monochromatic light emitting diodes (LED) with 360 nm and 620 nm wavelength, and a white LED. DC voltage in the range of -1.5 V to + 1.5 V has been applied to the devices to record the current conduction in dark condition as well as under the influence of the LEDs. In the experimental set-up, the distance between the devices are the LEDs were fixed at about 1 cm to ensure same intensity of LEDs in every experiment. The difference in the current conduction in the dark condition and under the LED light provide preliminary information about the photoactivity of the materials toward different monochromatic lights.

Electronic circuit fabrication for optoelectronic measurements

Previously, we developed circuits to generate electronic signals during the sensing applications. [51, 52] Such circuits are important for visual detection of the analyte present in liquid or gaseous state. Such devices are more practical to use and hence commercially available. In the current context, a different electronic circuit has been successfully designed as shown in the Scheme 2 for the optoelectronic measurements. The working mechanism of the circuit is explained below.

With reference to the scheme 2, the circuit was developed to find the efficiency of the photoactive material under light and dark conditions. For this, we need a light source of specific wavelength which remain ON and OFF state with definite adjustable time interval and here it is selected from 0.5 to 20 s. As mentioned earlier, monochromatic LEDs with 360 nm and 620 nm wavelength, and while LED were used for the experiments. The circuit was built around a timer IC NE555 followed by a dual Master–Slave JK Flip-flop IC 74LS73. The ON/OFF timing or output frequency of the IC 555 was designed as such so that it can be adjusted from 2 to 80 s with the help of 100 KΩ variable resistor. The output of IC 555 from pin 3 was then fed to IC 74LS73 in its pin number 5. IC 74LS73 then divide this input in to two equal part and thereby reducing its frequency by half and at the same time improves the quality of the wave front. Output of the 1st Master–Slave JK Flip-flop (pin 1) was then fed to the 2nd Flip-flop via pin number 9. So, after the 2nd Flip-flop we got a frequency exactly ¼ of the original wave front coming out from pin number 3 of the IC 555. One of the output from 2nd Flip-flop was fed into the base of the npn transistor BC547 via 330Ω resistor which in turn energies the 12 V relay with the help of the p-n-p power transistor BC368. So, with variation of the 100 KΩ variable resistance we can adjust the ON and OFF timing of the light source from 0.5 s to 20 s as required for our experiment.

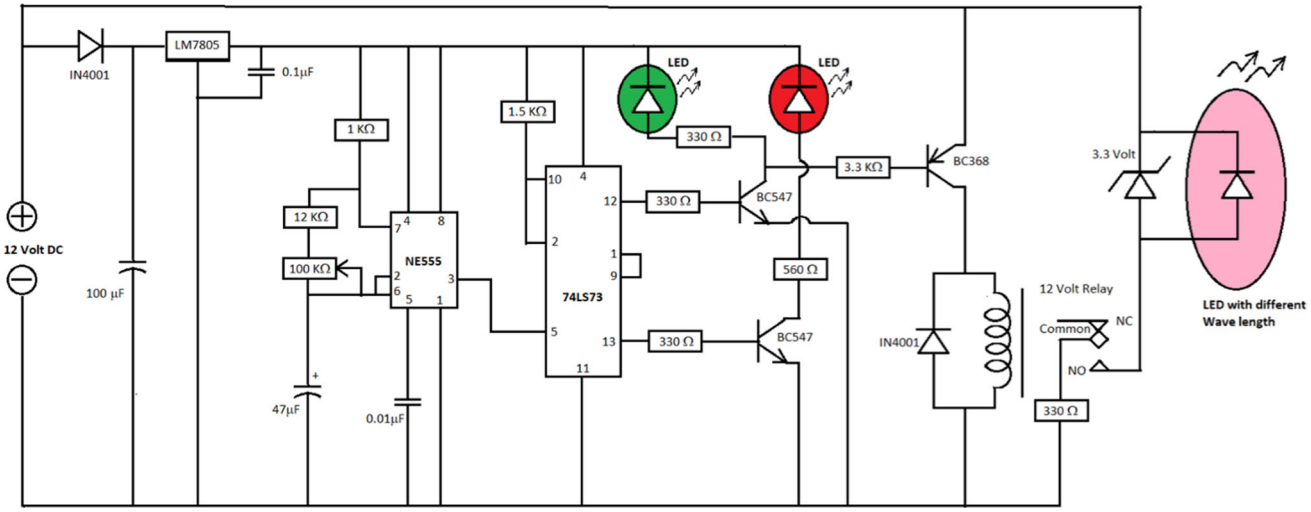

Scheme 2 Pictorial representation of the circuit developed for optoelectronic measurements.

Results and discussion

Material characterization

The degumming of silk fibers is explained in Sect. "Extraction of SF". The removal of the sericin protein has been confirmed with the help of SEM as shown in Fig. 1a, b. Here, Fig. 1a corresponds to the untreated silk fibers and the surface is significantly rough due to the presence of sericin protein as the outer layer. The degumming process results in the removal of the outer layer leaving behind the fibroin protein with a smooth surface as evident from Fig. 1b. To evaluate the uniformity of the degumming process, lower resolution SEM images (20 µm) are collected before and after the degumming process. As evident from the supplementary material Figure S1A-B, the surface of the silk fibers appears to be significantly smooth in a large surface area. It confirms complete removal of the sericin protein from the experimental silk fibers. The surface of the films deposited on PET substrates were also investigated under SEM as shown in Figure S1C-D. It was observed that, the roughness of the experimental film with 10% SF (V/V) and 8% PVA (W/V) is significantly lower than that of the SF alone.

The structural elucidation of SF has been done with the help of FT-IR spectral as shown in Fig. 2a. In the FT-IR spectra, the appearance of the bands at 1640 cm^{-1} (amide I), 1422 cm^{-1} (amide II), 1319 cm^{-1} (amide III) were characterized by β-sheet structure. The band near 3300 cm^{-1} represents for N–H stretching vibrations of amides [53]. Other peaks at 1008 cm^{-1} and 946 cm^{-1} are assigned due to the C-O stretching vibration and -OH out of plan bending vibration, respectively. [54] The UV–vis spectra of the SF protein in aqueous media possesses a strong band at 277 nm (Fig. 2b) and from the PL experiments at different excitation wavelength, we found that SF shows maximum emission when excited with 300 nm monochromatic light (Fig. 2c).

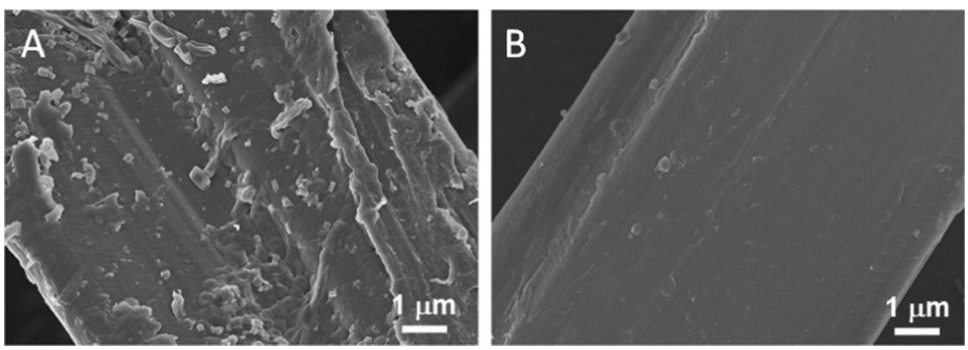

Figure 1 SEM images of **a** raw silk fiber, and **b** silk fiber after degumming.

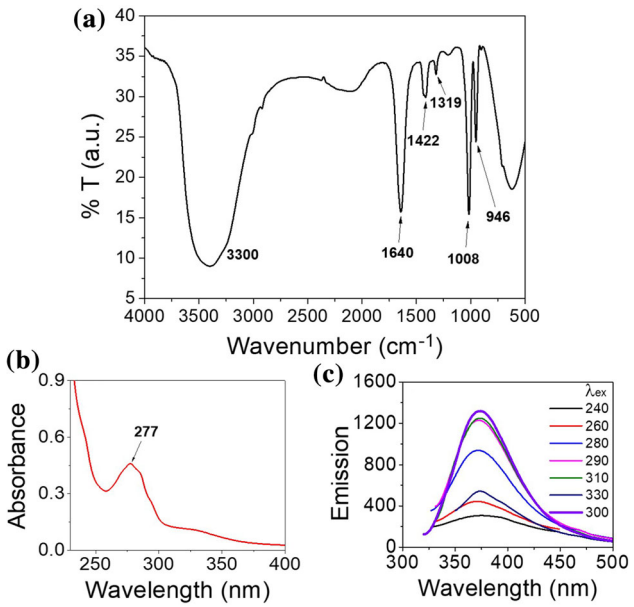

Figure 2 **a** FT-IR spectra of SF, **b** UV–vis spectra of SF, and C. PL spectra of SF at different excitation wavelength. 10% SF (V/V) solution was used for all the measurements, and at pH 7.

Sensing studies

Fluorescence measurements

The aqueous solution of SF is fluorescent in nature and shows emission maximum at about 370 nm when excited at 300 nm monochromatic wavelength (λ_{ex}). After the addition of PA into the SF solution, we observed a decrease in the fluorescence intensity of SF. With the increase in the concentration of PA (4.97, 9.9, 14.7, 19.6, and 24 nM), the fluorescence intensity of SF gradually decreases as shown in Fig. 3a, and at 24 nM of PA it undergoes about 74% fluorescence quenching. Similar results were obtained for the same stock solution of SF for a period of two months. After that, the solution is no longer stable to reproduce the results. From the calibration curve (Fig. 3b), the limit of detection (LOD) was calculated to be 0.203 nM of PA using the equation LOD = 3.3 σ/S, where, S is the slope of the plot and σis the relative standard deviation [55]. This value is lower than the recently reported fluorescence-based PA sensor in aqueous media. A comparative study is given in Sect. "Comparative study of the fluorescence measurements".

An ideal sensor must work in a real-world scenario and to achieve that the sensors has to be water soluble as all the sensing experiments are performed in aqueous media. Since SF is soluble in aqueous LiBr solution, it is possible to check its fluorescence response toward PA dissolved in tap-water and soil–water [7]. We found that, in both the cases SF undergoes about 93% quenching (Figure S2) at 30 nM of PA which is a clear indication that the material is useful in detecting PA in a much more complex environment than the controlled laboratory experiments. Additionally in real environmental solutions, there might be different other nitroaromatic compounds and ions at low concentrations which can alter the fluorescence quenching. It was observed that at the same concentration of 24 nM, other experimental nitroaromatic chemicals viz. ortho-, meta-, para-nitrophenol causes about 27.8%, 25.4%, and 28% decrease in the fluorescence, respectively, in comparison to 74% decrease by PA as mentioned earlier (Figure S3A). Additionally, in a mixture of all these experimental chemicals at the same molar ratios, 78% quenching was observed which is similar to the quenching efficiency for PA alone. The difference in florescence quenching for these experimental chemicals can be explained from the perspective of functional groups present in them. Due to the presence of one $-NO_2$ group and one –OH group, all these three nitrophenols can form hydrogen bonds with SF which can result into a small decrease in the

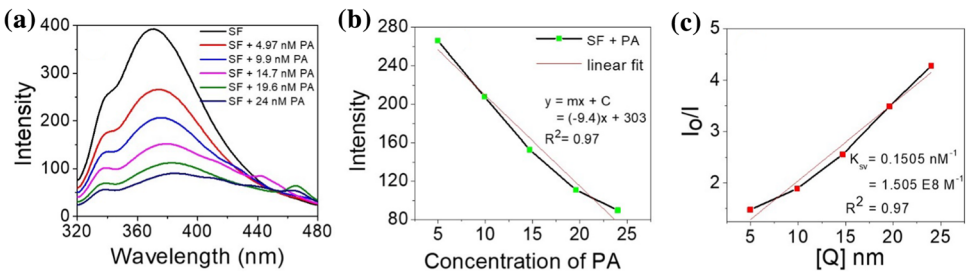

Figure 3 **a** Fluorescence spectra of 10% SF (V/V) solution in the presence of increasing concentration of PA, initial pH 6.5. **b** Calibration plot for determining the limit of detection, **c** Stern–Volmer plot with increasing concentration of PA.

fluorescence intensity of SF. However, the extent of hydrogen boning of SF with these chemicals is much weaker compared to that of PA with three $–NO_2$ groups and one –OH group. Therefore, it can be stated that the fluorescence quenching efficiency in the case of PA is higher among the experimental nitroaromatic analogues. We have also checked the fluorescence quenching of SF in the presence of same concentration of 1,10-phenanthroline, and interestingly it showed only about 1.2% fluorescence quenching to SF. Since, the chemical structure of 1,10-phenanthroline does not possess any $–NO_2$ group or–OH group, hydrogen bonding interaction is not possible with SF and hence it does not alter the fluorescence intensity of SF. For selectivity experiments, in addition to the other nitroaromatic analogues, it is also important to check the fluorescence of the sensors in presence of ions. It was observed that, the presence of common salts such as KCl, Na_2SO_4, and $ZnSO_4$, causes only about 4.8%, 3.3%, and 2.1% decrease in the fluorescence of SF, respectively (Figure S3A). This decrease in the fluorescence is negligibly small compared to that of the presence of PA. The quenching efficiency for all the experimental analytes is similar when SF was used after dialysis as shown in Figure S3B. Therefore, it can be said that the presence of LiBr use for the extraction of SF does not alter the efficacy of SF as sensor for PA. To mimic the interference of these nitroaromatic chemicals and different ions in real samples, we have checked the fluorescence response of SF toward PA in their presence in 1:1 ratio as shown in Figure S3C. Evidently, the interference of all the experiment chemicals is negligibly small.

In addition to the use of SF as a chemosensor in its polymeric form as extracted from silk fibers, we have further extended the sensing experiments by preparing fluorescent carbon dots (CDs) from SF using hydrothermal method [56]. These CDs also show undergo about 76% fluorescence quenching in the presence of 87 nM concentration of PA. The synthesis of CDs, their UV–Vis spectra and the fluorescence spectra at different excitation wavelengths, fluorescence sensing experiment are presented in the supplementary information (Figure S4).

To quantify the interaction between the fluorophore and the quencher and to predict the mechanism of fluorescence quenching, we have drawn the well-known Stern–Volmer (SV) plot from the fluorescence experiments.[57] The SV equation is expressed as:

$$I_0/I = 1 + K_{SV}[Q] \quad (1)$$

where, I_0 and I are the fluorescence intensities before and after the addition of the quencher [Q]. K_{SV} is the bimolecular binding constant. This equation predicts the occurrence of static or ground state stable complex formation or dynamic or excited state energy transfer quenching mechanism in the system. It represents a linear straight line and the slope of the plot provides the magnitude of $K_{SV.}$ Higher the magnitude of K_{sv}, better is the accessibility of the fluorophore to the quencher. [58] As evident from Fig. 3c, the SV plot of the system follows a nonlinear trend and the binding constant K_{SV} was calculated to be 1.505×10^8 M^{-1}, with a regression coefficient of 0.97. Such nonlinear SV plots indicate the presence of either the energy transfer mechanism in the excited state or the synergistic effect of ground state or excited state interaction mechanism. The general mechanisms involved in the fluorescence quenching are Förster resonance energy transfer (FRET), inner filter effect (IFE), photoinduced energy transfer (PET), and aggregation caused quenching (ACQ). In the present work, FRET is the main driving force for the quenching which has been confirmed with the help of experimental evidence. In the case of FRET, the analyte absorbs the light emitted by the fluorescent probe resulting in a fluorescence quenching. Therefore, the overlapping area of the emission spectra of the fluorophore and the UV–vis absorption spectra of the quencher provides the probability of FRET in between the two systems. In the case of SF as donor and PA as acceptor molecule, the mentioned spectral overlap is very prominent as shown in Fig. 4a. The calculated area of the overlapping region is about 72, which is significant for energy transfer. Additionally, the occurrence of FRET has been confirmed with the help of time resolved photoluminescence (TRPL) measurements as depicted in Fig. 4b and c. The energy transfer to the acceptor leads to the faster decay time for the combined system as compared to the donor alone [59]. The fluorescence lifetime (τ) of SF in aqueous media was found to be 4.26 ns, which decreases to 3.47 ns after the interaction with PA. Furthermore, the FRET efficiency can be obtained using the following equation:

$$E = 1 - (\tau_{DA}/\tau_D) \quad (2)$$

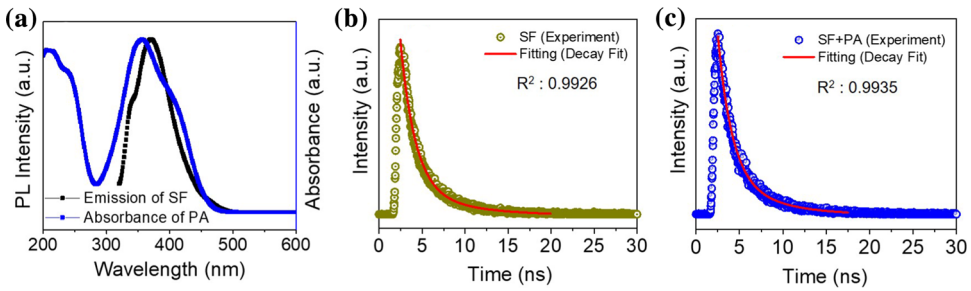

Figure 4 A. FRET: overlapping of the fluorescence spectra of 10% SF (V/V) solution and the UV–vis spectra of the PA. Time-resolved fluorescence decay profile of B. SF and C. SF + PA.

where, τ_D and τ_{DA} are the fluorescence lifetime of the donor and the donor–acceptor combination, respectively [60]. Using this equation, the FRET efficiency was found to be 0.185 (18.5%).

With reference to Fig. 5a and b, it can be stated that in addition to the FRET, the fluorescence quenching of SF is also supported by the hydrogen bonding interaction between SF and PA. Such interaction was previously reported by Dutta et al., and Sun et al.[52, 61] Due to the strong electron withdrawing effect of three nitro groups, the phenolic group of PA is highly acidic in nature and hence readily can form hydrogen bonding with the –OH as well as –NH groups of the SF. Similar nitroaromatic analogues such as ortho-, meta-, para-nitropheneol, do not have such highly acidic phenolic groups and hence their interaction with SF is expected to be weaker compared to that of PA alone. Hence, the fluorescence response of SF is highest in the case of PA. The occurrence of hydrogen bonding interaction is quite difficult to predict with the help of FT-IR spectroscopy as it produces broad spectra in the region 3400–3500 cm^{-1}. All the peak positions of SF remained intact after the indication with PA indicating no covalent interaction between SF and PA. Formation of covalent bonds would have led to a static interaction between them. This observation is in agreement with the TRPL results that confirm an energy transfer mechanism between the fluorophore and the quencher. Another probable mechanism associated with the FRET is the electrostatic interaction between SF and PA. For an efficient FRET to occur, the donor and the acceptor molecules must get sufficiently closer to each other, which apparently lead to electrostatic interactions between them. With the help of zeta potential (ζ) measurements in aqueous media as presented in the Figure S5, we found that the SF and PA possesses a surface charge of about −21.2 mV and -11.6 mV, respectively. The mixture solution of SF and PA possesses a cumulative ζ value of about −31.4 mV indicating a probable charge accumulation. This is a clear indication of the presence of electrostatic interaction between the donor and the acceptor. Therefore, we can conclude that the synergistic effect of FRET, hydrogen bonding and electrostatic interactions lead to a higher fluorescence quenching of the sensor system for PA. It would be interesting to investigate the electrical properties of these combined materials as such driving forces make significant contributions toward the change in the electrical properties of any system.

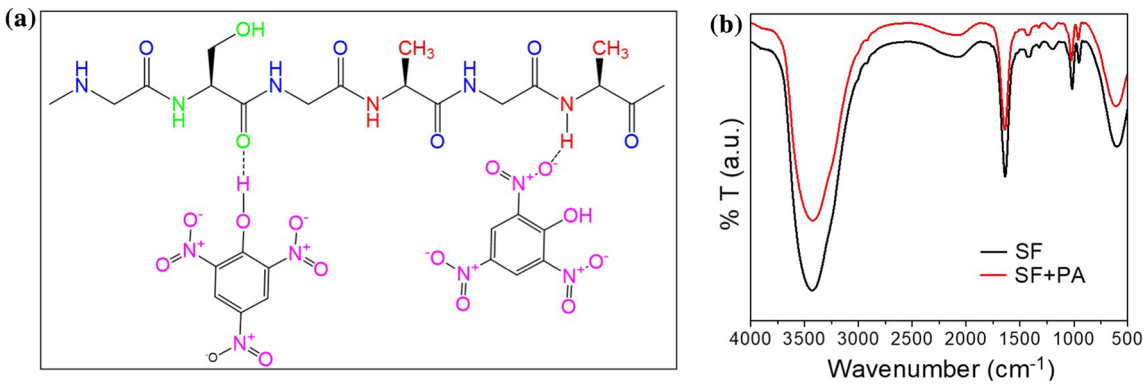

Figure 5 **a** Schematic representation of the hydrogen bonding interaction between SF and PA. **b** FT-IR spectra of SF before and after the sensing experiments.

Comparative study of the fluorescence measurements

From the materials perspective, for a selective and rapid sensing of PA in liquid media, materials have been synthesized in laboratories which may require different chemicals and have to go through different purification processes that require high purity solvent systems. These are time consuming and expensive processes. Accidental release of such synthetic materials to the environment also can cause environmental pollution and hence such materials have to be stored carefully for a longer duration. In such circumstances, it is pertinent to use biodegradable or biocompatible materials like SF protein which are as efficient as the synthesized materials in laboratories. Additionally, such biodegradable and biocompatible materials are abundantly available in nature and their extraction process is simple and straightforward making the whole process easy, less time consuming and inexpensive.

A comparative study of the efficiency of the SF with some of the recently reported picric acid sensors is presented in Table 1.

Electrical measurements

Electrical measurement-based sensing

All the electrical measurements for the sensing studies have been perfumed at ambient conditions and at 60% relative humidity (RH). As mentioned earlier, we designed flexible devices for sensing studies as well as to investigate the photoactivity of the materials. In the first case, SF mixed with 8% PVA (W/V) was drop casted on the PET substrate, while for the later the same mixture solution obtained from the fluorescence quenching experiments have been used. For the electrical sensing, 10 µL of 24 nM PA solution was added to the SF + PVA film in between the two silver electrodes (Fig. 6a) and then dried in a hot air oven. The *I-V* characteristics of the devices before and after adding PA was compared. A representative *I-V* plot of a device measured by applying AC bias voltage is shown in Fig. 6b. Evidently, the current conduction of the device increases after the addition of PA and at a maximum of 4 V, the device develops about twofold increase in the current conduction which is probably due to the high ionic nature of the PA. This has been confirmed by measuring the current response of the device at a constant DC applied voltage of 1 V with respect to time as shown in Fig. 6c, d. From this plot we have calculated the ionic transport number using the formula $(i_t\text{-}i_o)/i_o$, where i_o is the initial conduction and i_t is the current conduction when the device shows a constant steady current with respect to time. The ionic conduction of PVA + SF and PVA + SF + PA (24 nM) is 13% and 33%, respectively. The working principle of this experiment is that, under the influence of a DC bias, the ions of the materials get polarized and migrate toward the two silver (Ag) electrodes. So, initially, the current conduction is due to both the ionic and electronic migration (i_o). But the two Ag deposited on the PVA film act as ion blocking electrodes and hence the ionic migration occurs with time until a steady state is achieved (i_t). At this stage, the material is fully polarized and hence the residual current is mainly due to electronic movement. So, by using the mentioned formula the percentage ionic contribution toward the total conduction can be easily calculated.

To investigate the stability of the sensor, we have performed the fluorescence measurements after two months period of extracting the SF from the silk fibers. As shown in the Figure S6A, SF undergoes about 56% fluorescence quenching in presence of 24 nM of PA. Therefore, in aqueous media the quenching efficiency is lower compared to that of the freshly prepared SF. On the other hand, a flexible device stored in vacuum desiccator for two months was used for *I-V* measurement-based sensing of PA. The device developed twofold increase in the current conduction for 24 nM of PA as shown in the Figure S6B, which is similar to that of the freshly fabricated devices. From this observation, it can be stated that the sensor device is stable for two months.

Photoactivity of the materials

Photodetectors find a wide range of applications and hence should work in the real-world scenario such as varying RH as well as under mechanical stress. To investigate the capability of our material to work under such conditions, we have deposited the materials on flexible PET substrates and the impedance (Z) versus time were measured at higher bending angles, viz. 120° and 90°. The digital photograph of the device is shown in Fig. 7a. As evident from Fig. 7b, the log Z versus time plot of the device at 120° and 90° bending are in the same range with the normal condition, i.e. 180°. Also, the impedance

Table 1 Comparison of the present fluorescence sensor with recently reported picric acid sensor

Serial no.	Materials	Method	Medium	LOD	Refs.
1	Rhodamine-isonicotinic hydrazide	Fluorescence turn-on	Aqueous	37.3 nM	[62]
2	Dysprosium metal-organic framework	Fluorescence turn-off	Aqueous	0.71 μM	[63]
3	Polythiophene derivative	Colorimetric and fluorescence	Aqueous	50 nM	[64]
4	4,4′,4″,-(1.3.5-triazine-2.4.6-triyl)tris(N.N-diphenylaniline)	Fluorescence turn-off	Aqueous	0.37 nM	[65]
5	N′1, N′3-bis((E)-4- (diethylamino)-2 − hydroxybenzylidene)isophthalohydrazide	Fluorescence turn-on	95% aqueous media	12.15 nM	[66]
6	2, 6-bis (benzimidazolyl)-pyridine	Fluorescence turn on–off	Aqueous media	49.49 ppb	[67]
7	Functionalized pyrazoline derivative	Fluorescence turn off	THF–H_2O mixture	6.80×10^{-7} M	[68]
8	Benzimidazole-acrylonitriles	Fluorescence turn-on	Aqueous media	11-41μ M	[69]
9	Curcumin-cysteine and curcumin-tryptophan conjugate	Fluorescence turn-on	Aqueous media	13.51 nM	[7]
10	pyridyl-imine capped gold nanoaggregates	Fluorescence turn off	Aqueous media	15 nM	[70]
12	Anthracene-based fluorescent probe	Fluorescence turn-on	Aqueous media	30 ppb	[71]
13	poly(tannic acid) nanoparticles	Fluorescence turn off	Aqueous media	0.08 μM	[72]
11	SF protein	Fluorescence turn-off and *IV* measurements	Aqueous media	0.203 nM	Current work

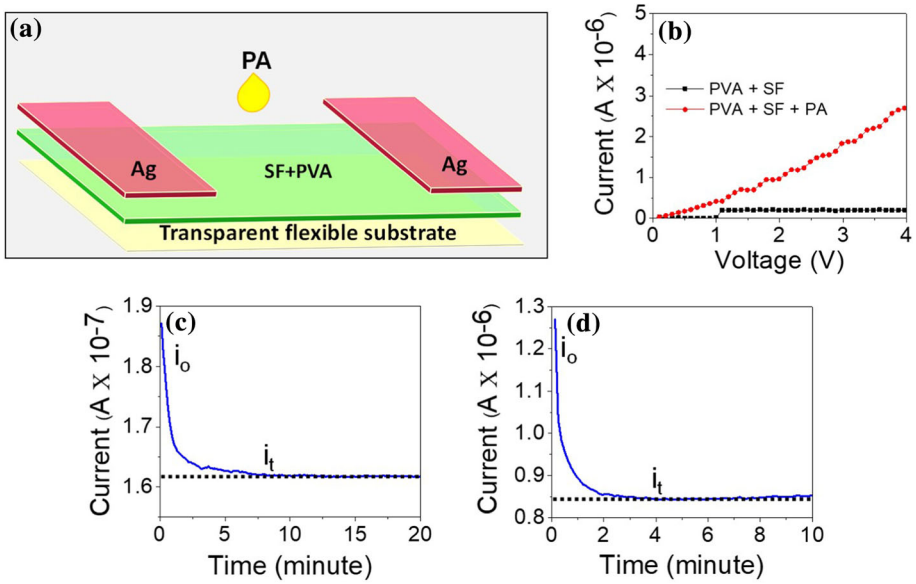

Figure 6 **a** Schematic representation of the device fabricated on flexible PET substrate for electrical measurements. **b** *I-V* characteristics of the device in the presence of 24 nM of PA. Current vs time plot of **c** SF + PVA, and **d** SF + PVA + PA (24 nM).

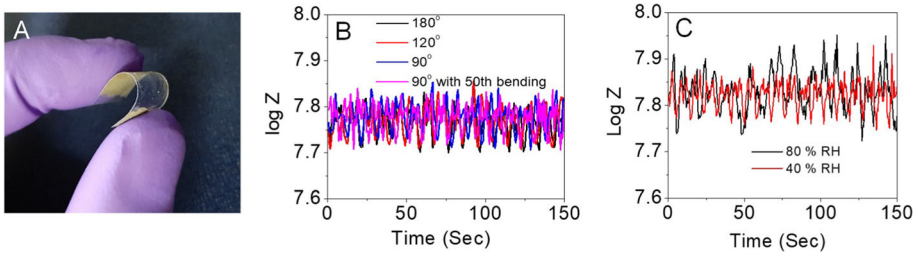

Figure 7 **a** Digital photograph of the flexible device fabricated on PET substrate. **b** Log Z versus time plot of the device at 180°, 120°, 90° angle of bending and also at 50th time bending to 90°. **c** Log Z versus time plot of the device at 80% and 40% relative humidity (RH).

response (log Z) remains in the same range even after bending the device to 90° for 50th time. From this observation it can be stated that, the photoactive material is useful at extremely high mechanical stress. This is particularly useful in designing wearable optoelectronic devices as well as applicable in real-world scenarios where external forces like accidental bending may cause a change in the shape of the device. Structural integrity of the photoactive material plays an important role in such experiments. Instead of using powdered photoactive materials or SF in its fiber form, we used the aqueous solution in combination with 8% PVA (W/V) which forms a stretchable film in the method that we employed. Such observations are not possible when solid substrates such as silicon wafers, ITO/FTO coated glass are used for device fabrication which are also known to be expensive. In the present case, under extreme bending angles, the network structure of the film is believed to be remained intact. This helps in retaining the original electrical properties in terms of log Z verses time. To support this observation, we have checked the surface roughness of the films before and after this set of experiments with the help of AFM measurements. It was found that the surface roughness of the material is similar and no cracked portions have been observed after the repeated bending of the device and after applying external bias voltages. The AFM images with the line profiles of the films are presented in Figure S7. Another important external parameter that has to be taken into account while studying optoelectronic properties is the effect of varying RH conditions toward the impedance response of the device. To investigate that, we have monitored the impedance response of the device at 80% and 40% RH. As shown in Fig. 7c, the impedance response (log Z) of the device with respect to time at the two RH conditions is in the same range indicating that the device can work under varying RH conditions in the laboratory.

Photoactivity of the materials were investigated by measuring the *I-V* characteristics of the devices in the external DC voltage range of −1.5 V to 1.5 V and under the irradiation of 360 nm, 620 nm and while LEDs. The device fabricated using the combination of PVA and SF + PA develops about 7.15 μA photocurrent under 360 nm wavelength monochromatic LED as depicted in Fig. 8a. While no such photocurrent generation has been observed for 620 nm and white light LEDs as evident from Fig. 8B-C. Similar to the PA sensing experiments in aqueous media, there is a significant spectral overlapping of the fluorescence spectra of SF with the absorption spectra of PA in 8% PVA (W/V) indicating the occurrence of FRET. In electrical measurements, FRET provides an effective charge carrier pathway in between the two materials, which facilitates the current conduction. In our system, the FRET comes into

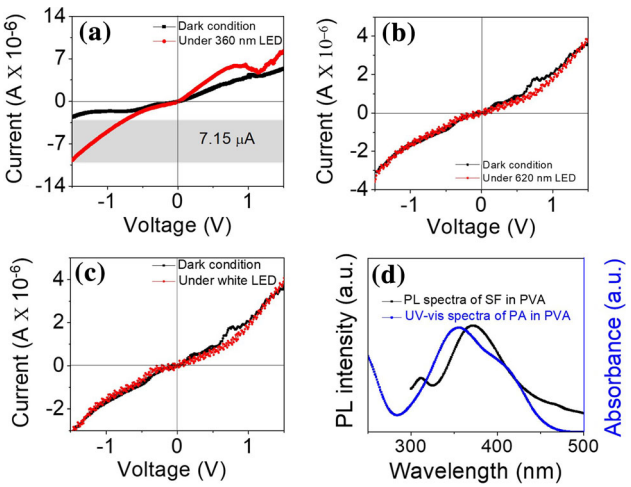

Figure 8 *I-V* characteristics of the Device-1 at **a** 360 nm LED, **b** 620 nm and **c** White light. **d** FRET: Spectral overlap between the UV–vis and the PL spectra of PA and SF protein in 8% PVA (W/V).

picture under the influence of 360 nm wavelength monochromatic LED and hence there is a significant increase in the photocurrent conduction. SF exhibits intrinsic protein fluorescence [48] and hence is a good candidate as donor molecule in the present system with a strong electron acceptor. The occurrence of FRET in between the donor–acceptor pair is evident from the large spectral overlapping as shown in Fig. 8d which is a major driving force toward the high photocurrent conduction at 360 nm monochromatic light. The integral area under the overlapping region was found to be about 85.19 that assess the efficacy of FRET between the two systems. Another cause of the higher current conduction is the increased ionic current due to the interaction between SF and PA. It is important to note that, PVA + SF protein or PVA + PA alone does not show any photocurrent under the same experimental conditions as shown in the supplementary information (Figure S8). It can be concluded that the presence of donor–acceptor energy transfer mechanism increase photoconduction by increasing the charge carrier generation and transport. Therefore, unlike the p-n heterojunction-based photodetectors, the devices work as a simple photoconductive photodetector.

To check the stability and long-term usability of the device, the *I-V* measurements of the same device have been done after three months using the same condition. After three months the photocurrent conduction was found to be about 6.7 μA (Figure S9). This value is similar to the result of its first measurement which indicates that the device is sufficiently stable for repetitive measurement. To develop a full-fledged photodetector and comprehensive analysis of the photodetector performance, it is important to determine the other device parameters such as responsivity, detectivity, response time, photoconductive gain [33]. The scope of the current work is only to develop a system applicable as a chemosensor and to find the signature characteristic feature of photoactive material simply by measuring the photocurrent developed under LED light irradiation. An attempt has been made to establish the underlying photophysical mechanisms and to investigate the factors that can alter the performance of the sensor and the devices.

Significance of the work

1. *Materials used:* Silk fibroin protein is an excellent biomaterial and its applications widely revolve around the biomedical applications, tissue engineering, etc. Its application as donor photoactive material required in optoelectronics as well as chemosensory material is not well explored. Since it's a biodegradable material, release of this material to the environment is not harmful.
2. *Simplicity of the method:* In terms of material synthesis, we have used a generalized and simple technique to extract silk fibroin protein from silk fiber and skipped the dialysis process required to remove the excess ions from the protein. This in a way reduces the cost of extracting the silk fibroin protein.

In terms of device fabrication, we have used a very straightforward technique to investigate the photocurrent developed in the combined system of silk fibroin protein and picric acid using PVA as a supporting materials by depositing the materials on PET flexible substrates. The devices show similar electrical properties with extreme bending angles and hence useful for fabricating wearable optoelectronic and biosensor devices in the future. Additionally, this device does not require an (ETL) and (HTL) which are widely used to increase the efficiency of the devices in general.

3. *Cost-effectiveness:* Use of naturally available materials, employing simple fabrication techniques without the use of expensive substrates and electron/hole transport layers, developing a versatile platform for chemosensing and photodetecion all together make the process cost-effective and yet viable.

Conclusion

SF protein has been introduced as a chemosensor for PA and photoactive material for developing UV photodetector. It was found that, SF undergoes efficient fluorescence quenching in the presence of nanomolar concentration of PA with a LOD as low as 0.203 nM which is considerably low compared to the previously reported fluorescence-based picric acid sensors. From the experimental evidence, we found that FRET between the sensor and the analyte is the

main reason behind the fluorescence quenching in the presence of PA. To further extend the observation for real environmental samples, we have investigated the fluorescence properties of SF protein for tap-water and soil-water. In both cases, the protein has shown about 93% decrease in fluorescence quenching. This indicates that the material is a potential candidate for the selective detection of nitroaromatic chemicals in real samples as well. On the other hand, SF is also a suitable material for fabricating portable electronic devices for chemosensing as well as for photodetection. We found that under 360 nm monochromatic LED, the device fabricated from the blended material of SF protein, PA and PVA develops about 7.15 μA photocurrent. Likewise the high fluorescence quenching in aqueous media, in the case of electrical measurements the FRET provides as additional pathway to facilitate charge transfer between the materials that increase the photocurrent generation. Moreover, varying relative humidity and different bending angles of the flexible devices do not alter their electrical properties. Furthermore, we have developed a low-cost electronic circuit for the current work as well as for future research. This is a necessary equipment used in studying the precise on–off characteristics and a controllable power supply to the LED to investigate different optoelectronic properties of devices. Our ongoing and future research focuses on developing fully operating and air-stable optoelectronics devices for long-term usability and also to study the underlying photophysical mechanisms of photoactive materials to enhance the efficacy of the devices.

Acknowledgements

This work is financially supported by the Department of Science and Technology (DST), Government of India under the DST INSPIRE Faculty scheme (IFA18-CH 313). BG is thankful to Department of Chemistry, Gauhati University, Guwahati for providing a laboratory as well as sophisticated instrumentation facilities. BG is also grateful to Prof. Neelotpal Sen Sarma for fabricating the electrical circuit. The authors thank Mr. Rakesh Talukder for collecting the SEM images.

Declarations

Conflicts of interest The authors declare no conflicts of interest.

Supplementary Information: The online version contains supplementary material available at https://doi.org/10.1007/s10853-021-06506-9.

References

[1] Ju KS, Parales RE (2010) Nitroaromatic compounds, from synthesis to biodegradation. Microbiol Mol Biol Rev 74:250–272

[2] Bhalla V, Gupta A, Kumar M, Rao DS, Prasad SK (2013) Self-assembled pentacenequinone derivative for trace detection of picric acid. ACS Appl Mater Interfaces 5:672–679

[3] Wyman JF, Serve MP, Hobson DW, Lee LH, Uddin DE (1992) Acute toxicity, distribution, and metabolism of 2, 4, 6- trinitrophenol (picric acid) in Fischer rats. J Toxicol Environ Health Part A 37:313–327

[4] Germain ME, Knapp MJ (2009) Optical explosives detection: from color changes to fluorescence turn-on. Chem Soc Rev 38:2543–2555

[5] McQuade DT, Pullen AE, Swager TM (2000) Conjugated polymer-based chemical sensors. Chem Rev 100:2537–2574

[6] Chen X, Sun C, Liu Y, Yu L, Zhang K, Asiri AM, Marwani HM, Tan H, Ai Y, Wang X, Wang S (2020) All-inorganic perovskite quantum dots $CsPbX_3$ (Br/I) for highly sensitive and selective detection of explosive picric acid. Chem Eng J 379:122360

[7] Gogoi B, Sarma NS (2015) Curcumin–cysteine and curcumin–tryptophan conjugate as fluorescence turn on sensors for picric acid in aqueous media. ACS Appl Mater Interfaces 7:11195–11202

[8] Lee YH, Liu H, Lee JY, Kim SH, Kim SK, Sessler JL, Kim Y, Kim JS (2010) Dipyrenylcalix [4] arene—a fluorescence-based chemosensor for trinitroaromatic explosives. Chem Eur J 16:5895–5901

[9] Koh LD, Cheng Y, Teng CP, Khi YW, Loh XJ, Tee SY, Low M, Ye E, Yu HD, Zhang YW, Han MY (2015) Structures, mechanical properties and applications of silk fibroin materials. Prog Polym Sci 46:86–110

[10] Nguyen TP, Nguyen QV, Nguyen VH, Le TH, Huynh VQN, Vo DVN, Trinh QT, Kim SY, Le QV (2019) Silk fibroin-

based biomaterials for biomedical applications: a review. Polymers 11:1933

[11] Khalid A, Bai D, Abraham A, et al. (2020) Electrospun nanodiamond-silk fibroin membranes: a multifunctional platform for biosensing and wound healing applications. arXiv preprint ar Xiv:2006.00614.

[12] Patil PP, Reagan MR, Bohara RA (2020) Silk fibroin and silk-based biomaterial derivatives for ideal wound dressings. Int J Biol Macromol 164:4613–4627

[13] Zhang H, Liu Y, Chen C, Cui W, Zhang C, Ye F, Zhao Y (2020) Responsive drug-delivery microcarriers based on the silk fibroin inverse opal scaffolds for controllable drug release. Appl Mater Today 19:100540

[14] Asadpour S, Kargozar S, Moradi L, Ai A, Nosrati H, Ai J (2020) Natural biomacromolecule based composite scaffolds from silk fibroin, gelatin and chitosan toward tissue engineering applications. Int J Biol Macromol 154:1285–1294

[15] Zhao Z, Xu C, Niu L, Zhang X, Zhang F (2020) Recent progress on broadband organic photodetectors and their applications. Laser Photonics Rev 14:2000262

[16] Omnès F, Monroy E, Muñoz E, Reverchon JL (2007) Wide bandgap UV photodetectors: a short review of devices and applications. Gallium Nitride Materials and Devices. Int Soc Op Photonics 6473:277–786

[17] Lan Z, Lei Y, Chan WKE, Chen S, Luo D, Zhu F (2020) Near-infrared and visible light dual-mode organic photodetectors. Sci Advances 6:eaaw065

[18] Chahrour KM, Yam F, Abdalrheem R (2019) High-performance UV photodetector of anodic rutile TiO_2 nanotube arrays. Mater Lett 248:161–164

[19] Gedamu D, Paulowicz I, Kaps S, Lupan L, Wille S, Haidarschin G, Mishra YK, Adelung R (2014) Rapid fabrication technique for interpenetrated ZnO nanotetrapod networks for fast UV sensors. Adv Mater 26:1541–1550

[20] Li Y, Huang W, Liu H, Wang J, Tian L, Zhang S (2018) UV photodetector based on polycrystalline SnO_2 nanotubes by electrospinning with enhanced performance. J Nanopart Res 20:334

[21] Dong Y, Wang S, Zou Y, Liu S, Zhu Z, Li J, Ju D, Chen J, Zhang K, Liu X, Zeng H (2018) Zinc stannate nanocrystal-based ultrarapid-response UV photodetectors. Adv Mater Technol 3:1800085

[22] Huang PH, Shen YC, Tung CY, Huang CY, Tan CS, Horng RH (2020) Energy-saving $ZnGa_2O_4$ phototransistor improved by thermal annealing. ACS Appl Electron Mater 2:3515–3521

[23] Han X, Feng S, Zhao Y, Li L, Zhan Z, Tao Z, Fan Y, Lu W, Zuo W, Fu D (2019) Synthesis of ternary oxide Zn_2GeO_4 nanowire networks and their deep ultraviolet detection properties. RSC Adv 9:1394–1402

[24] Chen D, Xin Y, Lu B, Pan X, Huang J, He H, Ye Z (2020) Self-powered ultraviolet photovoltaic photodetector based on graphene/ZnO heterostructure. Appl Surf Sci 529:147087

[25] Wang F, Gao T, Zhang Q, Hu ZY, Jin B, Li L, Zhou X, Li H, Tendeloo GV, Zhai T (2019) Liquid- alloy- assisted growth of 2D ternary $Ga_2In_4S_9$ toward high- performance UV photodetection. Adv Mater 31:1806306

[26] Wang H, Wang X, Luo X, Song W, Guo J, Sun Y, Zhang B, Wang L, Zhang X, He L, Zhang K, Li S (2019) Optimization of all figure-of-merits in well-aligned GaN microwire array based Schottky UV photodetectors by Si doping. ACS Photonics 6:1972–1980

[27] Liang S, Dai Y, Wang G, Xia H, Zhao J (2020) Room-temperature fabrication of SiC microwire photodetectors on rigid and flexible substrates via femtosecond laser direct writing. Nanoscale 12:23200–23205

[28] Zhang Y, Ji T, Zhu J, Zou R, Hu J (2020) A high performance self-powered heterojunction photodetector based on NiO nanosheets on an n-Si (100) modified substrate. Mater Lett. p 128995

[29] Tu W, Liu T, Zhang Z, Wu G, Chen H, Wang M (2016) Ultra-wide bandgap organic acceptor material and its application in organic UV photodetector. Synth Met 219:20–25

[30] Murad AR, Iraqi A, Aziz SB, Abdullah SN, Brza MA (2020) Conducting polymers for optoelectronic devices and organic solar cells: a review. Polymers 12:2627

[31] Fernández IV, Mariotti S, Hutter OS, Birkett M, Veal TD, Hobson TDC, Phillips LJ, Danos L, Nayak PK, Snaith HJ, Xie W, Sherburne MP, Asta M, Durose K (2020) Vacancy-ordered double perovskite Cs_2TeI_6 thin films for optoelectronics. Chem Mater 32:6676–6684

[32] Li Y, Zhang X, Huang H, Kershaw SV, Rogach AL (2020) Advances in metal halide perovskite nanocrystals: synthetic strategies, growth mechanisms, and optoelectronic applications. Mater Today 32:204–221

[33] Hussain AA (2020) Constructing caesium-based lead-free perovskite photodetector enabling self-powered operation with extended spectral response. ACS Appl Mater Interfaces 12:46317–46329

[34] Lu L, Pan X, Luo J, Sun Z (2020) Recent advances and optoelectronic applications of lead- free halide double perovskites. Chem Eur J 26:16975–16984

[35] Nie R, Sumukam RR, Reddy SH, Banavoth M, Seok SI (2020) Lead-free perovskite solar cells enabled by heterovalent substitutes. Energy & environmental science. Energy Environ Sci 13:2363–2385

[36] Hussain AA, Rana AK, Ranjan M (2019) Air-stable lead-free hybrid perovskite employing self-powered photodetection with an electron/hole-conductor-free device geometry. Nanoscale 11:1217–1227

[37] Fernández S, Molinero A, Sanz D, González JP, Cruz M, Gandía JJ, Cárabe J (2020) Graphene-based contacts for optoelectronic devices. Micromachines 11:919

[38] Lee DH (2020) Synthesis and fabrication of graphene-based organic transparent electrodes for flexible optoelectronic devices

[39] Wang J, Song J, Mu X, Sun M (2020) Optoelectronic and photoelectric properties and applications of graphene-based nanostructures. Mater Today Phys 13:100196

[40] Essner JB, Baker GA (2017) The emerging roles of carbon dots in solar photovoltaics: a critical review. Environ Sci Nano 4:1216–1263

[41] Jiang X, Huang W, Wang R, Li H, Xia X, Zhao X, Hu L, Chen T, Tang Y, Zhang H (2020) Photocarrier relaxation pathways in selenium quantum dots and their application in UV-Vis photodetection. Nanoscale 12:11232–11241

[42] Thakur MK, Fang CY, Yang YT et al (2020) Microplasma-enabled graphene quantum dot-wrapped gold nanoparticles with synergistic enhancement for broad band photodetection. ACS Appl Mater Interfaces 12:28550–28560

[43] Venettacci C, García BM, Prato M, Moreels I, Lacovo AD (2019) Increasing responsivity and air stability of PbS colloidal quantum dot photoconductors with iodine surface ligands. Nanotechnology 30:405204

[44] Lin KC, Huang PR, Li H, Cheng H, Chang GE (2021) Temperature-dependent characteristics of GeSn/Ge multiple-quantum-well photoconductors on silicon. Opt Lett 46:3604–3607

[45] Cao R, Wang HD, Guo ZN, Zhang LY, Xiao QL, Zhang YP, Fan DY, Li JQ, Zhang H (2019) Black phosphorous/indium selenide photoconductive detector for visible and near-infrared light with high sensitivity. Adv Op Mater 7:1900020

[46] Liu J, Li Y, Song Y, Ma Y, Chen Q, Zhu Z, Lu P, Wang S (2017) Bi_2Te_3 photoconductive detectors on Si. Appl Phys Lett 110:141109

[47] Johnston ER, Miyagi Y, Chuah JA, Numata K, Serban MA (2018) Interplay between silk fibroin's structure and its adhesive properties. ACS Biomater Sci Eng 4:2815–2824

[48] Amirikia M, Shariatzadeh SMA, Jorsaraei SGA, Mehranjani MS (2018) Auto-fluorescence of a silk fibroin-based scaffold and its interference with fluorophores in labeled cells. Eur Biophys J 47:573–581

[49] Kalita B, Gogoi B, Sarma NS (2019) Cholesterol-aminoacid conjugates treated filter paper- based photoluminescence indicator for nitroaromatic chemicals. Mater Res Bull 115:211–218

[50] Mazzi S, Zulker E, Buchicchio J, Anderson B, Hu X (2014) Comparative thermal analysis of Eri, Mori, Muga, Tussar silk cocoons and fibroin fibers. J Therm Anal Calorim 116:1337–1343

[51] Gogoi B, Paul N, Chowdhury D, Sarma NS (2015) Instant detection of picric acid vapour 635 by developing layer by layer polymer detectors and an electronic prototype. J Mater Chem C3:11081–11089

[52] Dutta P, Saikia D, Adhikary NC, Sarma NS (2015) Macromolecular systems with MSA-Capped CdTe and CdTe/ZnS Core/Shell quantum dots as superselective and ultrasensitive optical sensors for picric acid explosive. ACS Appl Mater Interfaces 7:24778–24790

[53] Zhang YQ, Shen WD, Xiang RL, Zhuge LJ, Gao WJ, Wang WB (2007) Formation of silk fibroin nanoparticles in water-miscible organic solvent and their characterization. J Nanopart Res 9:885–900

[54] Pavia DL, Lampman GM, Kriz GS, Vyvyan JA (2014) Introduction to spectroscopy

[55] Gogoi B, Sarma NS (2015) Poly-glycerol acrylate and curcumin composite: its dual emission fluorescence quenching and electrical properties for sensing 2-vinyl pyridine. J Mater Sci 50:7647–7659

[56] Wang Q, Cai J, Biesold-McGee GV, Huang J, Ng YH, Sun H, Wang J, Lai Y, Lin Z (2020) Silk fibroin-derived nitrogen-doped carbon quantum dots anchored on TiO_2 nanotube arrays for heterogeneous photocatalytic degradation and water splitting. Nano Energy 78:105313

[57] Chakravarty S, Gogoi B, Mandal BB, Bhardwaj N, Sarma NS (2018) Silk fibroin as a platform for dual sensing of vitamin B_{12} using photoluminescence and electrical techniques. Biosens Bioelectron 112:18–22

[58] F Teale (1984) MACMILLAN MAGAZINES LTD PORTERS SOUTH, 4 CRINAN ST, LONDON, ENGLAND N1 9XW,

[59] Paterson KA, Arlt J, Jones AC (2020) Dynamic and static quenching of 2-aminopurine fluorescence by the natural DNA nucleotides in solution. Methods App Fluoresc 8:025002

[60] Gupta V, Bharti V, Kumar M, Chand S, Heeger AJ (2015) Polymer–polymer förster resonance energy transfer significantly boosts the power conversion efficiency of bulk-heterojunction solar cells. Adv Mater 27:4398–4404

[61] Sun X, Ma X, Kumar CV, Lei Y (2014) Protein-based sensitive, selective and rapid fluorescence detection of picric acid in aqueous media. Anal Methods 6:8464–8468

[62] Sakthivel P, Sekar K, Singaravadivel S, Sivaraman G (2019) Rhodamine- isonicotinic hydrazide analogue: a selective fluorescent chemosensor for the nanomolar detection of picric acid in aqueous media. Chem Select 4:3817–3822

[63] Rajak R, Saraf M, Verma SK, Kumar R, Mobin SM (2019) Dy (iii)-Based metal–organic framework as a fluorescent probe for highly selective detection of picric acid in aqueous medium. Inorg Chem 58:16065–16074

[64] Zhang L, Sun Y, Jiang Y, Li Y, Song G, Huang K, Yao Z (2020) Visual sensing of picric acid in 100% aqueous media based on supramolecular polythiophene assemblies with colorimetric and fluorescent dual response. Chin Chem Lett 31:2428–2432

[65] Sathiyan G, Balasubramaniam B, Ranjan S, Chatterjee S, Sen P, GargcA GRK, Singh A (2019) A novel star-shaped triazine- triphenylamine–based fluorescent chemosensor for the selective detection of picric acid. Mater Today Chem 12:178–186

[66] Sharma S, Dubey G, Sran BS, Bharatam PV, Hundal G (2019) Fabrication of a Hydrazone based Al (III)-selective "turn-on" fluorescent chemosensor and ensuing potential recognition of picric acid. ACS Omega 4:18520–185209

[67] Jiang K, Chen SH, Luo SH, Pang CM, Wu XY, Wang ZY (2019) Concise design and synthesis of water-soluble fluorescence sensor for sequential detection of Zn (II) and picric acid via cascade mechanism. Dyes Pigm 167:164–173

[68] Guo S, Zhang Y, Huang J, Kong L, Yang J (2021) High dual-state blue emission of a functionalized pyrazoline derivative for picric acid detection. Cryst Eng Comm 23:221–226

[69] Jana P, Yadav M, Kumar T, Kanvah S (2021) Benzimidazole-acrylonitriles as chemosensors for picric acid detection. J Photochem Photobiol Chem 404:112874

[70] Singh G, Saini V, Lal G, Saraiya A, Singh N (2021) Tripodal pyridyl-imine capped gold nano-aggregates for selective detection of picric acid in aqueous media. Mater Sci Eng B 264:114970

[71] Duraimurugan K, Harikrishnan M, Madhavan J, Seung AS, Lee JL, Theerthagiri J, Choi MY (2021) Anthracene-based fluorescent probe: Synthesis, characterization, aggregation-induced emission, mechanochromism, and sensing of nitroaromatics in aqueous media. Environ Res 194:110741

[72] Zhao Y, Xu L, Kong F, Yu L (2021) Design and preparation of poly (tannic acid) nanoparticles with intrinsic fluorescence: a sensitive detector of picric acid. Chem Eng J 416:129090